J. Mat. NanoSci. 2024, 11(1), 952 Article

Journal of
Materials NanoScience

Biological and electrochemical Sensor detection studies of ZrO_2 wrapped by reduced Graphene Oxide nanocomposite

Sanjeevarayappa C[1], Nagegowda P[2], Mylarappa M[3*], Chandruvasan S[4], Sandhya R[5], Prassana Kumar S G[6]

[1]Department of Chemistry, Government First grade College, Yelahanka, Karnataka, India. [2]Department of Chemistry, Government First grade College, Channapatna, Karnataka, India. [3]Department of Studies in Chemistry, Bangalore University, Bengaluru, Karnataka, India. [4]Department of Chemistry, KLE Society's S Nijalingappa College, Rajajinagar, Bengaluru, Karnataka, India. [5]Department of Studies in Chemistry, Karnatak University, Pavate nagar, Dharwad, Karnataka, India. [6]Department of Chemistry, M S Ramaiah College of Arts, Science and Commerce, Bengaluru, Karnataka, India.

Submitted on: 07-Jun-2024 Accepted and Published on: 15-Jul-2024

ABSTRACT

The present work reports synthesis of ZrO_2 nanoparticles wrapped by reduced graphene doped (rGO) nanosheet through simple reflux method. The sample was characterized using XRD, FE-SEM, EDAX, FTIR, UV-Visible techniques. The optical bandgap was calculated using Tauc's method and found to be ZrO_2 and ZrO_2/rGO are 1.47 and 1.25 eV, respectively. The prepared rGO/ZrO_2 was established over anti-fungal, anticancer, and antioxidant studies. Anti-fungal activity against *Penicillium sp.* and *Aspergillus Niger* shows the enhanced zone of inhibition in both fungal species at increased concentration of ZrO2 and ZrO2/rGO samples. *Penicillium sp.* displays greater inhibition zones in both samples compared to Aspergillus Niger. The anticancer activity of ZrO_2/rGO conjugated with doxorubicin exhibit comparable activity on HeLa cells. The sample shows 82% free radical scavenging activity using 2,2-diphenylpicrylhydrazyl (DPPH) free radical, with IC_{50} value of 31 mg/mL. The electrochemical techniques were assessed to know the capacitance and sensing performance against lysine sensor. There has been a significant improvement in electrochemical behavior such as specific capacitance (C_{sp}), diffusion coefficient (D) and sensing behavior and shows better sensing properties using prepared material.

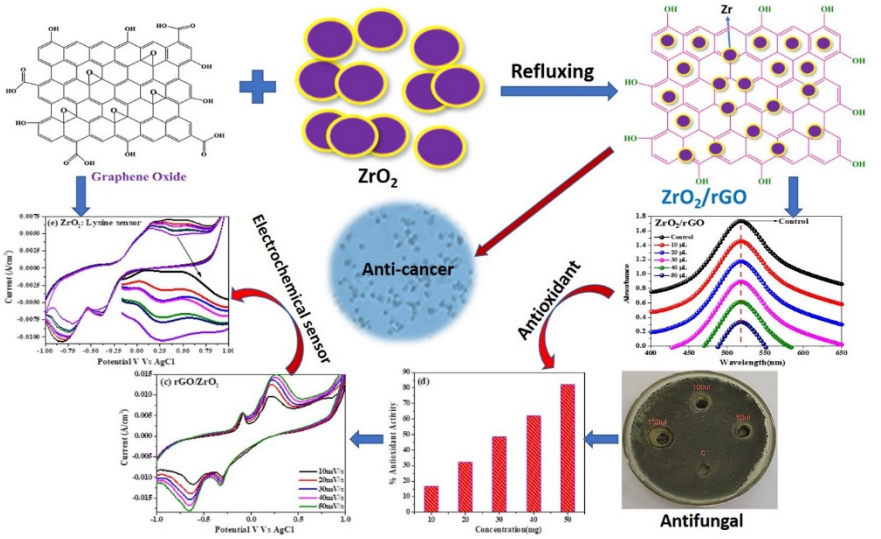

Keywords: rGO, ZrO2/rGO, Biological, Electrochemical, Sensor studies

INTRODUCTION

Recently, a variety of graphene-related materials, such as graphene oxide (GO), reduced graphene oxide (rGO), and reduced graphene oxide nanocomposites (rGO/NCS), have demonstrated potential in various biomedical applications [1]. Graphene's exceptional electrical, mechanical, thermal, and optical properties stem from its two-dimensional (2D) honeycomb lattice composed of sp^2 hybridized carbon atoms. Moreover, graphene exhibits biodegradability, cytocompatibility, and a substantial surface area [2-3]. Beyond its intriguing properties, graphene has emerged as a viable drug delivery platform for anti-cancer therapies. This capability allows it to selectively release pharmaceuticals to targeted cancer cells, a feature that is particularly exciting [4]. Graphene and graphene oxide have recently garnered significant

*Corresponding Author: Dr. M Mylarappa
Address: Bangalore University, Bengaluru, Karnataka, India.
Tel: +91-97424-13751; Email: mylu4mkallihatti@gmail.com

Cite as: *J. Mat. NanoSci., 2024, 11(1), 952.*

attention for their potential medical applications. However, there remains limited understanding regarding the toxicity or biological interactions associated with these materials. To ensure the safe and effective utilization of reduced graphene oxide (rGO) materials at cell interfaces, it is imperative to establish controlled biological interactions [5]. Currently, the gold standard for assessing the cytotoxicity of nanocomposite materials involves conducting in vitro research. Numerous in vitro studies have explored graphene's toxicity across various cell types, including HeLa, ovarian cancer, MCF-7 (human breast cancer), SKBR3, primary mouse embryonic fibroblast, NIH3T3, PC12 (derived from pheochromocytoma), and HepG2 cell lines [6]. The standard procedures for rGO-based cell toxicity experiments typically involve assessing parameters such as plasma membrane damage, reduced mitochondrial function, DNA damage, induction of oxidative stress, and ultimately, determining whether cell death occurs via necrosis or apoptosis [7-8]. However, contradictory data exist, particularly with graphene oxide (GO), due to variations in cell line sensitivity to nanomaterials and the inherent characteristics of the analysed nanomaterials. Generally, the type of reducing agent used and the resulting particle size determine the biocompatibility and cytotoxicity of reduced graphene oxide nanocomposites (rGO NCs) [9].

Nanostructures composed of metal oxides exhibit several advantageous electrical and optical characteristics, including a high surface-to-volume ratio, modified surface work function, enhanced catalytic activity, and the capability to capture phonons and electrons [10].

ZrO_2 nanoparticles (NPs) are regarded as environmentally friendly and potentially beneficial biological agents because of their outstanding chemical inertness and low toxicity [11]. ZrO_2 nanoparticles (NPs) possess favourable attributes that render them exceptional materials for numerous catalytic and sensing applications [12-14], as well as various biological systems such as plants and microbes. These properties encompass biocompatibility, thermal stability, and cost-effectiveness in manufacturing. Notably, sulfated ZrO_2 NPs demonstrated significant effects when evaluated for toxicity against colon and liver cancer cells [15]. Furthermore, studies have reported the impact of ZrO_2 NPs on the development of the Pseudomonas putida bacterium strain [16-17]. Mogha et al. described a biocompatible ZrO_2/rGO nanocomposite, which they utilized as a biosensor for the chemical chlorpyrifos [18]. Sai Saraswathi et al. [19] illustrated the cytotoxic effects of ZrO_2 NPs on MCF-7 cell lines. Balaji et al., utilizing the DCFH2-DA dye assay, showcased the cytotoxicity of ZrO_2 NPs on HCT-116 and A549 cell lines, proposing a mechanism of action. Further substantiation of ZrO_2 NPs' cytotoxicity towards cancer cell lines surfaced, implicating reactive oxygen species (ROS) as the causative agent [20]. The authors meticulously outlined the chemical pathway involved in reactive oxygen species (ROS) production, oxidative stress, and subsequent cell death induced by nanoparticles [21-22]. Graphene, acting as an electron acceptor, inhibited the recombination of electron-hole pairs, thereby amplifying ROS generation [23]. The cytotoxicity, DNA damage, apoptosis, and cancer induced by nanomaterials all stem from this fundamental process [24]. Various techniques are available for synthesizing ZrO_2/rGO nanocomposites, including hydrothermal methods, electrochemical synthesis, and solution-based approaches [25-26]. However, these documented methods often require extreme heat, prolonged reaction times, high pressure, and the generation of undesired by-products. Additionally, for large-scale synthesis operations, most of these approaches involve synthesizing ZrO_2 nanoparticles and reduced graphene oxide separately before combining them in a solution [27-28]. Here, work describe synthesis of ZrO_2 decorated on rGO sheet and categorizations through XRD, FE-SEM, EDAX, FTIR and UV-Vis spectroscopy. The synthesized ZrO_2/rGO was used to explore the biological and electrochemical sensor studies.

MATERIALS AND METHODS

Hydrogen peroxide (H_2O_2), Zirconyl Nitrate ($ZrO(NO_3)_2.H_2O$), Tri-Sodium citrate ($Na_3C_6H_5O_7$), Sulphuric acid (H_2SO_4), Sodium sulphite (Na_2SO_3), Sodium nitrate ($NaNO_3$), Potassium permanganate ($KMnO_4$) and ethyl alcohol (C_2H_5OH). These materials were purchased from the Merck and were utilized in the experiment in their original.

Preparation of RGO

The rGO was prepared by modified hummer's method was reported in the literature by Mylarappa et al. [29-30].

Preparation of rGO Synthesis of ZrO_2 and ZrO_2/rGO

Weigh 0.25 g of rGO was dispersed in 50 mL of distilled water and subjected to ultra-sonication for 4 hours. Then 0.75 g of ZrO_2 was added to the mixture and stirred using a magnetic stirrer. After 1hr. had passed, sodium citrate (1g) was boiled for a duration of 100 minutes, and approximately 3 g of sodium sulphite was prepared in 25 mL of deionized water then added into the solution and stirred for 4 hours at a temp. of 100°C. Subsequently, the mixture was allowed to cool, and filtered. The obtained product was washed several times with deionized water. The product was dried at 700 °C using muffle furnace [31]. Similarly, ZrO_2 was prepared through same procedure, without the addition of rGO, same amount of precursor and reagents were used to prepare zirconium oxide (ZrO_2) and the material was calcined at 700 °C.

RESULTS AND DISCUSSION

XRD

The X-ray diffraction (XRD) was employed to examine the crystalline nature of the synthesized ZrO_2 and ZrO_2-rGO as shown in the Fig.1. As per the JCPDS card file no. 79-1771, the diffraction peaks were observed in the ZrO_2/rGO nanocomposite at 2 theta angles of 30, 35, 50, 60, 62 and 74°, corresponding to the (101), (110), (200), (211), (202) and (220) crystal planes [32]. Additionally, a second diffraction peak with a (002) plane was observed at 26.5° (JCPDS no. 75-1621), indicating the presence of reduced graphene oxide [33]. The Debye-Scherer equation (1) was utilized to determine the size of ZrO_2 nanoparticles deposited on the rGO sheets.

$$d = \frac{k\lambda}{\beta\cos\theta} \dots\dots\dots\dots\dots\dots\dots (1)$$

In this equation, d represents the particle size, while k serves as a dimensionless shape factor with a typical value around 0.9. The variable λ stands for the wavelength of the incident radiation, typically X-rays in X-ray diffraction experiments. β denotes the

line broadening in radians at half maximum intensity (FWHM), which characterizes the breadth of diffraction peaks in the XRD pattern. Lastly, θ represents the Bragg angle, the angle at which the X-rays are diffracted by the crystal lattice. By utilizing the Debye-Scherrer Equation (1), the particle size corresponding to the (101) plane was determined to be 23.56 nm.

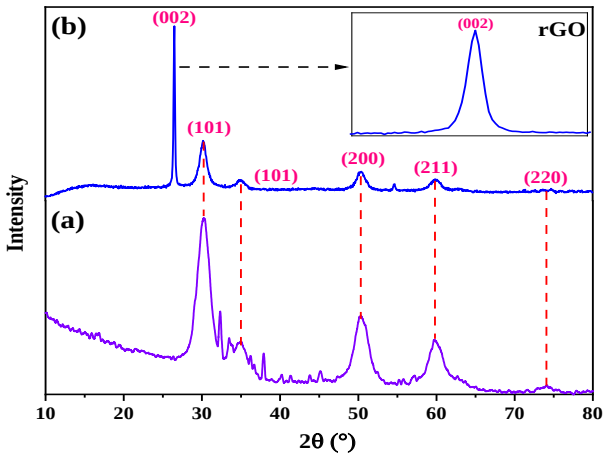

Figure 1. The XRD spectra of (a) ZrO_2 and (b) ZrO_2/rGO.

FE-SEM

The field emission scanning electron microscopy (FE-SEM) was employed to study the surface morphology of ZrO_2 and ZrO_2/rGO as shown in the Fig.2. In Fig. 2(a) zirconium spherical shaped particles are well settled on the surface of rGO sheets and also particles are overstocked with each other [34]. In Fig. 2(b) image shows particles are scattered throughout the sheets of reduced graphene sheets, this shows an effective formation of ZrO_2/rGO through simple reflux method [35]. The energy dispersive X-ray analysis (EDAX) was employed to study the composition of and ZrO_2/rGO as shown in the Fig. 2 (c). The EDAX data analysis reveals the weight percentage of Zr (29.09%), C (19.6%) and O (51.28%) respectively. This elemental distribution (Zr, C, O) provides favourable evidence for the successful fabrication of the ZrO_2/rGO nanocomposite [36-37].

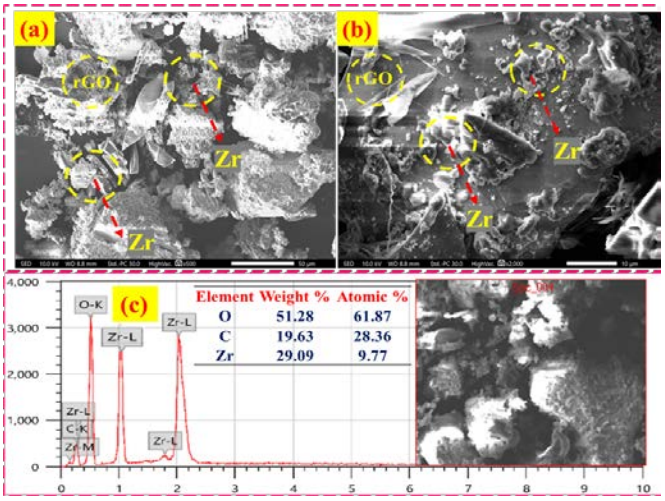

Figure 2. The FE-SEM image of (a, b) ZrO_2/rGO and EDAX spectrum of (c) ZrO_2/rGO.

FTIR

Fig. 3 shows the functional group identification of ZrO_2 and ZrO_2/rGO using Fourier transform infrared spectroscopy (FTIR). In Fig. 3(a), the FTIR spectra of ZrO_2 nanoparticles are presented. Noticeable, robust peaks at 3418 and 1624 cm^{-1} were attributed to the stretching and bending vibrations of the -OH groups of adsorbed water. The presence of a peak at 1430 cm^{-1} suggests the existence of hydrated molecules, possibly in the form of hydroxyl groups. Additionally, the distinctive tetragonal Zr-O vibration occurs at 680 cm^{-1}, and the broadness of the band indicates that the ZrO_2 powders are nano-crystalline [38]. When rGO and ZrO_2 nanocomposites are combined, a hetero-junction forms, causing the Zr-O bond's stretching vibration to shift slightly to the lower frequency range, between 764 cm^{-1} and 658 cm^{-1}. In the FTIR spectra, there is no identifiable peak in the fingerprinting region when rGO is considered alone. The results depicted in Figure 3(b) indicate a strong interaction between the ZrO_2 and rGO compounds, as reported previously [39].

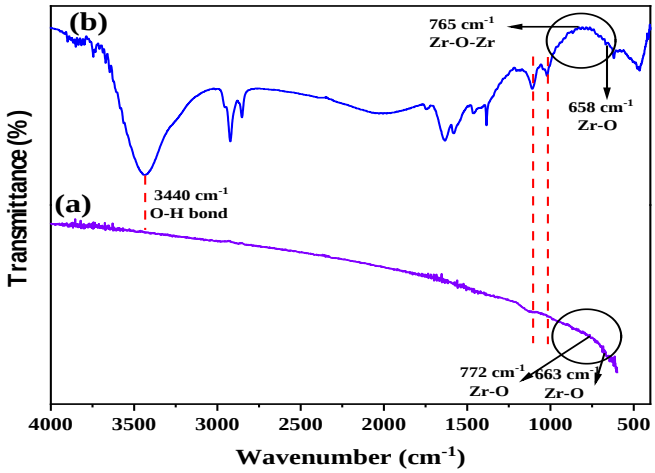

Figure 3. The FTIR spectrum of (a) ZrO_2 and (b) ZrO_2/rGO.

UV-Vis and Tauc's Plot

The Ultra violet visible spectroscopy and Tauc's plot was employed to study the absorbance and band gap analysis of ZrO_2 and ZrO_2/rGO shown in the Fig. 4(a-b). This analysis test method appears to be highly sensitive, yielding rapid reactions and accurate detection of nanoparticle/nanocomposite formation in the UV range spanning from 200 to 1000 nm. According to UV-Vis peaks, absorbance peaks were identified at 263 nm for ZrO_2 [40] and 268 nm for the ZrO_2/rGO nanocomposite. Therefore, the results clearly demonstrate the confirmation of nanoparticle and nanocomposite formation throughout the process.

To determine the energy band gap, the Kubelka-Munk function was utilized, which was employed in Tauc's relation (Eq. (3) [42]) and in Eq. (2) to obtain the absorption spectra.

$$F(R)=\frac{1-R^2}{2R} \qquad (2)$$

$$(\mathbf{F(R)h\nu})^2 = \mathbf{C(h\nu - Eg)} \qquad (3)$$

Here, 'E_g' represents the energy band gap, 'C' denotes a constant, and "hυ" signifies the energy of a photon. The value of $(F(R)h\upsilon)^2$ is

calculated using Eq. (3). At the inflection point, a tangent to $(F(R)h\upsilon)^2 = 0$ is drawn, and the optical band gap is determined by plotting $(h\upsilon)$ versus $(F(R)h\upsilon)^2$. The band gaps for ZrO_2 and ZrO_2/rGO are 1.47 and 1.25 eV, respectively, as depicted in Fig. 4 (inset) (a) and (b).

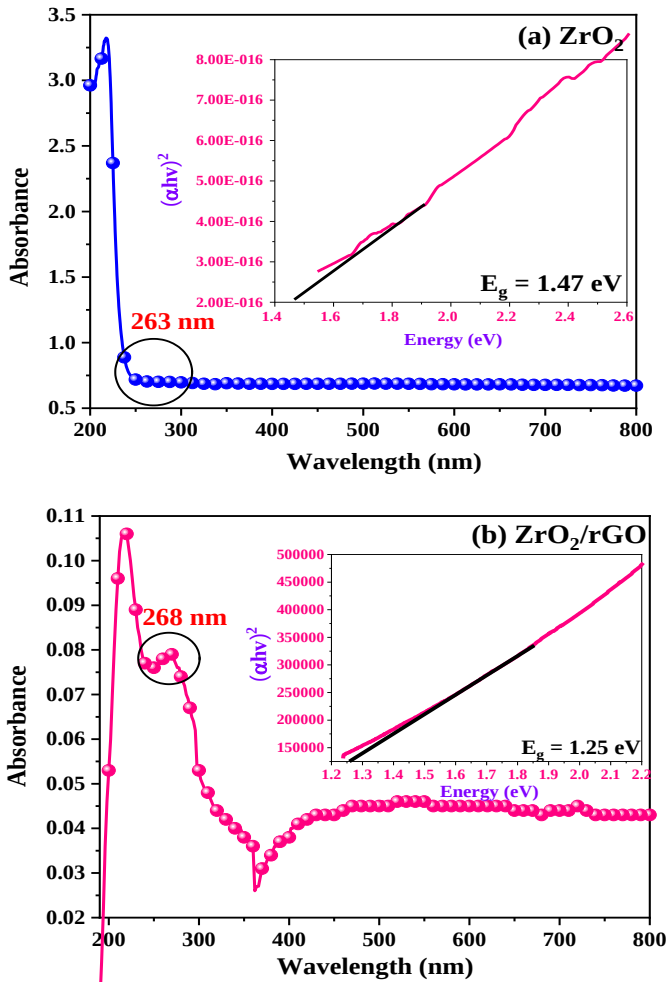

Figure 4. The UV absorption and Tauc's plot spectra (inset) of (a) ZrO_2 and (b) ZrO_2/rGO.

Anti-fungal studies

Fig. 5 shows the antifungal activity of ZO (ZrO_2) and RZ (ZrO_2/rGO) samples against *Penicillium sp* and *Aspergillus niger* was investigated using the disc-diffusion method. The *Penicillium* shows a zone of inhibition for ZO sample (0.2, 0.4 and 0.6 mm) and RZ shows a zone of inhibitions (0.3, 0.4 and 0.7 mm). The other fungal species *Aspergillus niger* was shown at 0.1, 0.2 and 0.3 mm for ZO and 0.2, 0.3 and 0.5 mm for RZ sample as shown in the Fig.6 (a) and 6 (b). A control sample of chloramphenicol was utilized for this study but does not show any zone of inhibition in both samples as indicated in Table 1. The zone of inhibition was increased in both fungal species at increased concentrations (50, 100, 150 µL) of ZO and RZ. *Penicillium sp.* shows higher inhibition zones in both samples compared to *Aspergillus niger*.

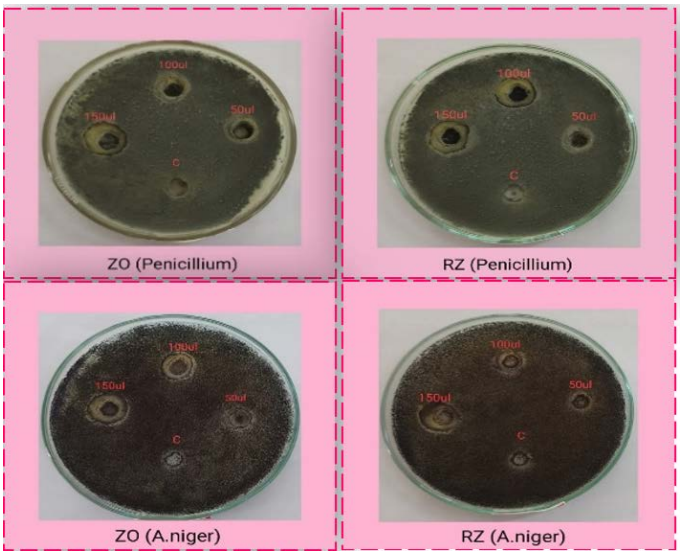

Figure 5. Anti-fungal activity of ZO and RZ samples *Penicillium sp.* and *Aspergillus Niger*.

Table 1. Anti-fungal activity against *Penicillium sp.* and *Aspergillus Niger*.

Samples	Zone of Inhibition (mm)					
	ZO			RZ		
Conc. (µL)	50	100	150	50	100	150
Penicillium sp.	0.2	0.4	0.6	0.3	0.4	0.7
Aspergillus Niger	0.1	0.2	0.3	0.2	0.3	0.5

Note: Control (C) = 0 mm

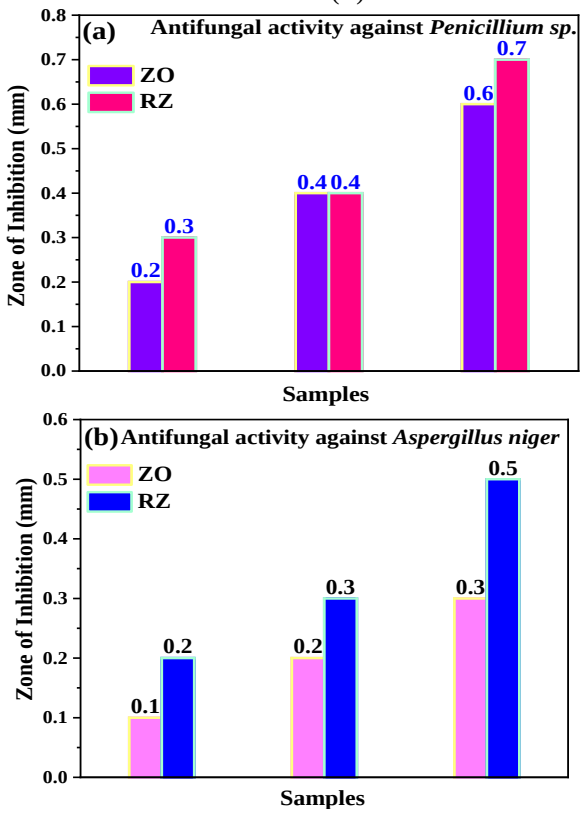

Figure 6. Zone of Inhibition graph of ZO and RZ (a) *Penicillium sp.* (b) *Aspergillus Niger*.

Anti-cancer studies

The HeLa cells used in this study were obtained from the National Cell Science Centre in Pune. The cell culture growth media consisted of DMEM medium supplemented with 10% fetal bovine serum, 100 µg/mL penicillin, and 100 µg/mL streptomycin. The cells were cultivated in a controlled atmosphere with 95% air and 5% CO_2 at a temperature of 37°C. Upon the formation of a monolayer of cells on the flask, they were then transferred to a new culture vessel. The cells were dissociated by exposing them to trypsin-EDTA (0.25% trypsin with 0.01% EDTA) for a duration of 5 minutes. Subsequently, media were added to halt the dissociation process. The cell viability was evaluated using the MTT (dimethylthiazol-diphenyltetrazolium bromide) reduction assay. HeLa cells were seeded onto a 96-well microtiter plate at a concentration of 1 x 10^5 cells/mL. Subsequently, the cells were incubated at 37°C with 5% CO_2 for 24 hours to facilitate attachment to the bottom of the wells. Prior to application to the microtiter plate, each extract/drug was prepared as a stock solution at a conc. of 1 mg/mL. The extract was diluted sequentially to achieve conc. ranging from 1-100 µg/mL and 24-hour incubation period was allotted for the microtiter plate. Control wells were populated with cells treated with 2% DMSO (Dimethylsulfoxide). Subsequently, the cells were exposed to MTT (5 mg/mL) for a duration of 4 hours. After dissolving the dark blue formazan crystals produced within viable cells using DMSO. The absorbance was measured at a wavelength of 570 nm using a Tecan 1650 model ELISA plate reader. The results were presented as a percentage of MTT reduction relative to the absorbance of control cells.

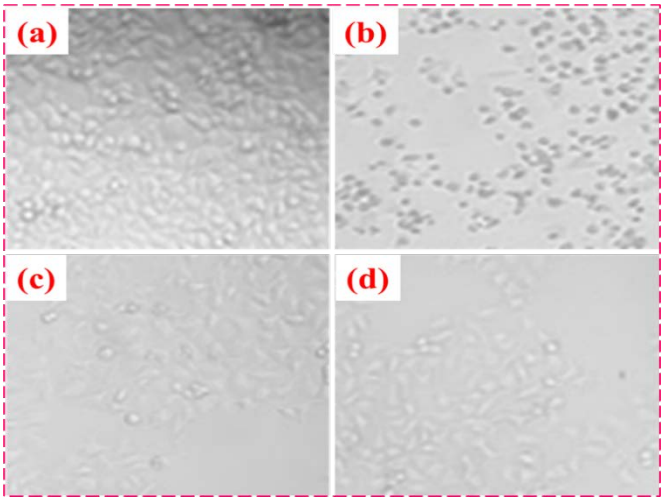

Figure 7. Anti-cancer effects of ZO and RZ (100µg/mL) against HeLa cells (a) Control cells (b) Doxorubicin treated (c) ZO treated (d) RZ treated.

Table 2. The Anti-cancer studies of ZO and RZ samples with different concentration.

Samples	Conc. (µg/mL)						
	1	2.5	5	10	25	50	100
	Cell Viability (%)						
Doxorubicin	96.64	82.49	77.49	68.45	55.38	37.85	25.03
ZO	92.29	93.34	84.74	83.28	72.16	71.83	60.14
RZ	99.31	92.31	87.63	85.65	79.19	72.45	66.56

HeLa cells were subjected to treatment with various drugs (ZO and RZ) at different concentrations (1, 2.5, 5, 10, 25, 50, 100 µg/mL) to assess their impact on cell viability. Among the tested concentrations, the highest concentration of 100 µg/mL demonstrated notable anticancer activity, resulting in cell viability percentages of 66% and 67% for ZO and RZ samples as indicated in Table.2. In comparison, the standard drug doxorubicin exhibited a cell viability of 25% at the highest concentration tested. These results suggest that ZO and RZ have shown significant anticancer potential activity at higher concentrations and more efficiency of the standard drug in inhibiting cell growth in HeLa cells shown in the Fig.7.

Antioxidant studies

To evaluate the antioxidant capacity, the DPPH free radical The antioxidant activity of ZrO_2 and ZrO_2/rGO samples against the DPPH free radical, a scavenging method was employed. A stock solution of 50 mg/mL was prepared by dissolving 50 milligrams of the sample in 50 mL of water. Dissolve 0.002 g of DPPH in 50 mL of ethanol and the resulting solution was applied to the samples in various doses subsequent to the initial combination of DPPH and methanol. After 1-hour of incubation at 25°C, measure the absorbance at 517 nm using a UV-Vis spectrophotometer. To achieve a 50% reduction in free radicals, it was imperative to ascertain precise time intervals and estimated concentrations for each portion. The assessment of antioxidant effects involved separating the solution into 5 individual test tubes each volume ranging from 10 to 50 µL. Add methanol carefully into each test tube using a micropipette and ensuring even distribution. Before covering the test tubes with aluminum foil, add 0.5 mL of the DPPH solution to prevent evaporation. Allow the mixture to stand for at least 1- hour after mixing and then UV equipment was used for further analysis. Eq. (4) was employed for conducting the evaluation of antioxidant activity.

$$\% \, D = \frac{A_c - A_s}{A_c} \times 100 \qquad (4)$$

Where "A_s and A_c" represents the absorbance of the sample and control. Tables 3 and 4 outline the specific procedures for calculating the IC_{50} value and assessing antioxidant activity. In Fig. 8 (a and c) and Fig. 8 (b and d) depict the respective UV spectra and percentage antioxidant properties of ZrO_2 and ZrO_2/rGO. The radical scavenging activities of ZrO_2 (78.07 mg/mL) and ZrO_2/rGO nanocomposite (31.061 mg/mL) are indicated in Tables 3 and 4. Indeed, achieving an optimal antioxidant activity is desirable, typically indicated by a lower IC_{50} value. The IC_{50} value, which indicates the concentration at which a substance neutralizes half of the free radicals, serves as a crucial metric for assessing the efficacy of materials in scavenging free radicals. Upon interaction with ZrO_2 and ZrO_2/rGO, the free radical DPPH in the methanol solution readily accepted an electron, leading to its transformation into a stable molecule and subsequent loss of its characteristic pink color. This visually observable decolorization serves as a direct indicator of the effective antioxidant activity exhibited by these materials.

Table 3. IC_{50} values and Antioxidant activity of ZrO_2.

Sample (µL)	Ethanol (µL)	Conc. (µg)	Absorbance	% Activity	IC_{50} (mg/mL)
10	50	10	1.62	6.35	
20	40	20	1.51	12.71	78.07
30	30	30	1.39	19.65	
40	20	40	1.3	24.85	
50	10	50	1.17	32.36	
Control			1.73		

Table 4. IC_{50} values and Antioxidant activity of ZrO_2/rGO.

Volume (µL)	Ethanol (µL)	Conc. (µg)	Absorbance	% Activity	IC_{50} (mg /mL)
10	50	10	1.44	16.76	
20	40	20	1.17	32.36	
30	30	30	0.89	48.55	31.061
40	20	40	0.66	61.84	
50	10	50	0.31	82.08	
Control			1.73		

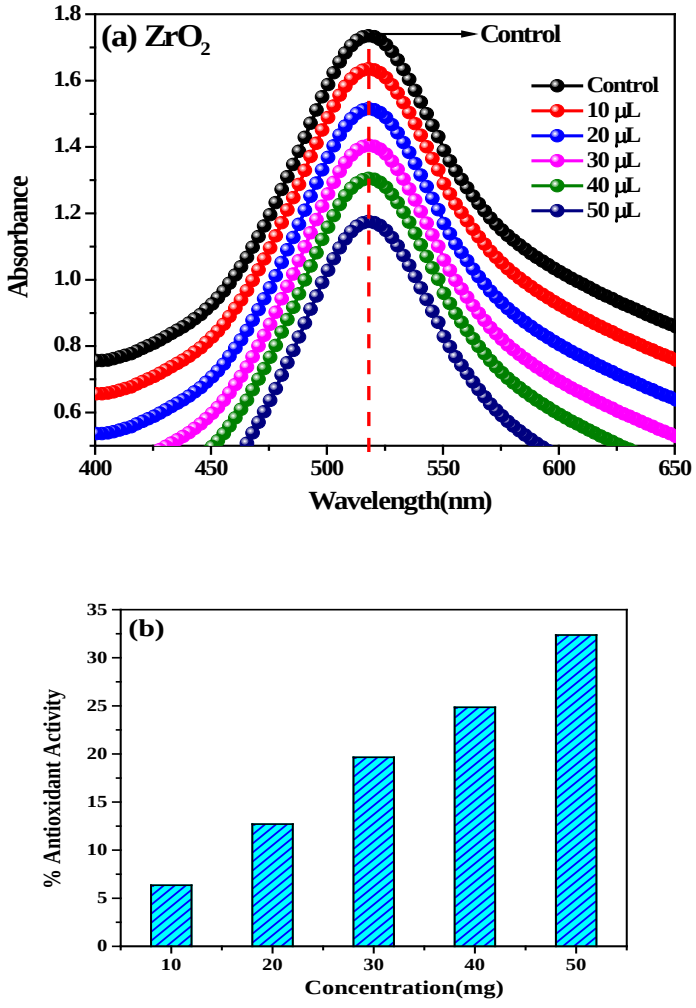

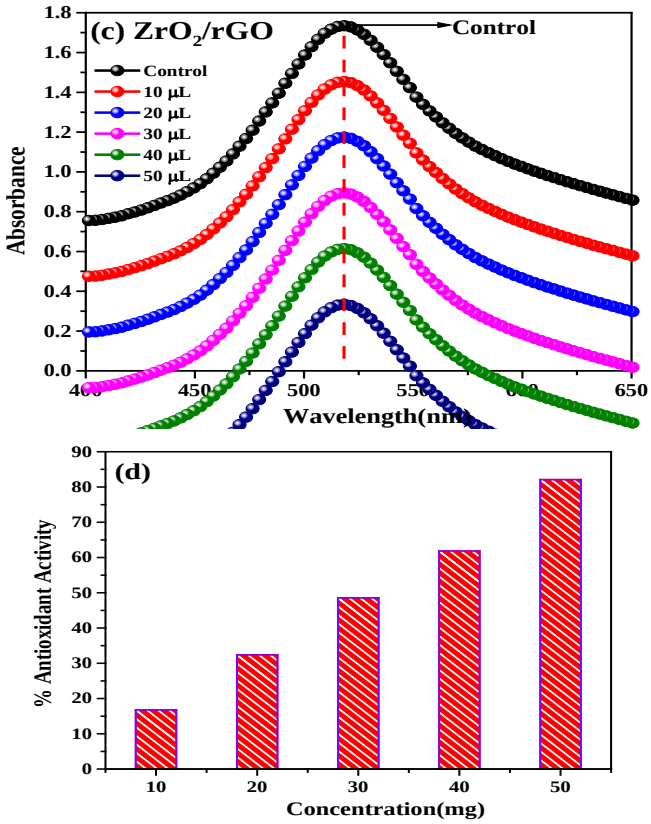

Figure 8. (a, c) UV graph and (b, d) % AA of ZrO_2 and ZrO_2/rGO.

CYCLIC VOLTAMMETRY AND ELECTROCHEMICAL SENSOR STUDIES

The Cyclic voltammetry and electrochemical studies were done by using Nickel mesh electrode was reported by Mylarappa et al [34]. The impressive electrical connection and expansive surface area of graphene have garnered significant interest within the electrochemical sensor sector. Researchers have been investigating electrode materials for biosensors and electrochemical sensors, which include rare earth metal oxides like ZrO_2. One major obstacle to the broad adoption of ZrO_2 nanomaterials is their limited electrical conductivity. A feasible approach has been discovered to enhance the catalytic activity of hybrid composite electrode materials. This method involves augmenting graphene and other materials possessing a significant surface area and exceptional conductivity by incorporating metal oxide nanoparticles.

The complementary actions of graphene and metal oxides may result in increased sensitivity and selectivity for electrochemical sensors. The relationship obtained from the cyclic voltammetry (CV) approach in Eq. (5) was used to calculate the specific capacitance of ZrO_2 and ZrO_2/rGO [30].

$$C_{sp} = \frac{A}{2ms(V_2 - V_1)} \dots\dots\dots\dots\dots (5)$$

The surface area (A), mass of active material (m), scan rate (s), final and initial potential windows (V_2 and V_1), and scan rate (s) were found to correlate with the specific capacitance (C_{sp}) of ZrO_2/rGO. Higher specific capacitance values denote an enhanced

capacity for energy storage. The reversibility and diffusion coefficients of the ZrO_2 and ZrO_2/rGO electrode were analyzed through cyclic voltammetry (CV) in a 0.1 KOH electrolyte over the potential range of -1.0 to 1.0 V, as depicted in Fig. 9(a and c). In Fig. 9(b and d), the proton diffusion coefficient, Slope and R^2 value are tabulated in the readings in Table 5 and 6.

Table 5. Reversibility and diffusion coefficient of ZrO_2.

Scan rate (mV/s)	E_O	$-E_R$	E_O-E_R	D	C_{sp} F/g
10	0.00348	0.00457	0.00805		
20	0.00542	0.00632	0.01174		
30	0.00884	0.00807	0.01691	0.0022	126
40	0.00939	0.00918	0.01857	-0.0017	
50	0.01235	-0.0118	0.02415		

Table 6. Reversibility and diffusion coefficient of ZrO_2/rGO.

Scan rate (mV/s)	E_O	E_R	E_O-E_R	D	C_{sp} F/g
10	0.00972	-0.01185	0.02157		
20	0.0125	-0.01399	0.02649		
30	0.0137	-0.01542	0.02912	0.0013	238
40	0.0144	-0.01697	0.03137	-0.0016	
50	0.0149	-0.01816	0.03306		

As chemical sensors lysine was detected using the ZrO_2 and rGO/ZrO_2 electrode's cyclic voltammetry (CV) measurement. Lysine can be detected by the Nickel mesh electrode ZrO_2 in an acidic solution (0.1 M KCl) for amounts ranging from 1 to 5 mM, as shown by a substantial change in the reduction current from -0.15 to -0.65 V in Fig. 9 (e). Likewise, as illustrated in Fig. 9(f), the sensor detects Lysine in 0.1 M KOH across various concentration ranges from 1 to 5 mM, within the reduction potential from -0.25 to -0.85 V. The produced electrode in the 0.1 M KOH solution shows improved sensor detection when Lysine is present. Furthermore, the sensor has a low reversibility curve, indicating that it works better in terms of reversibility than the other ZrO_2 electrode [31].

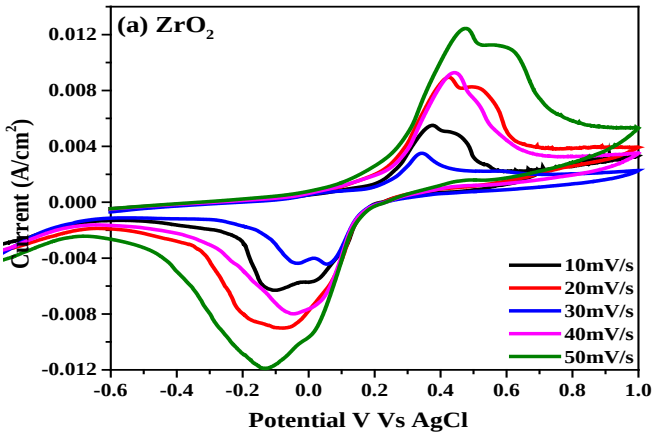

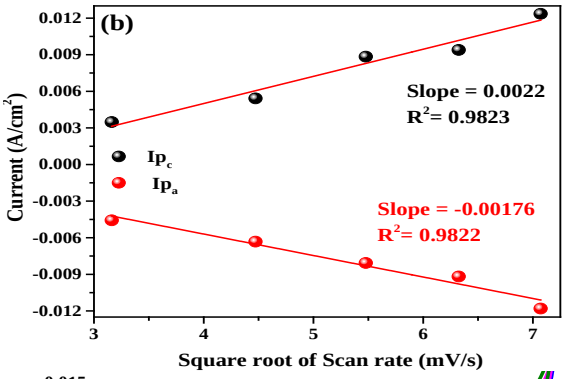

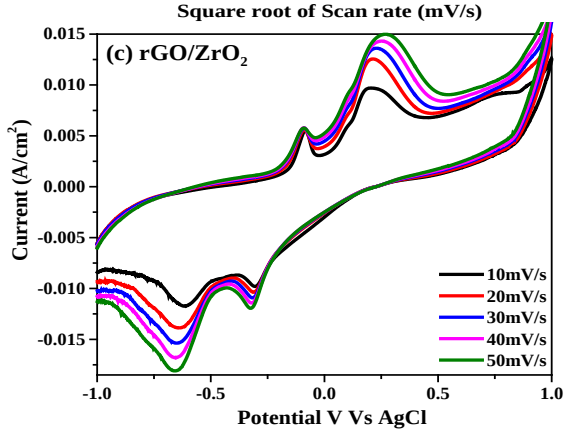

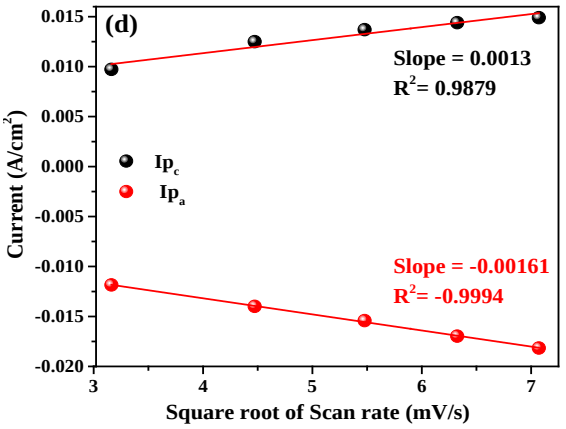

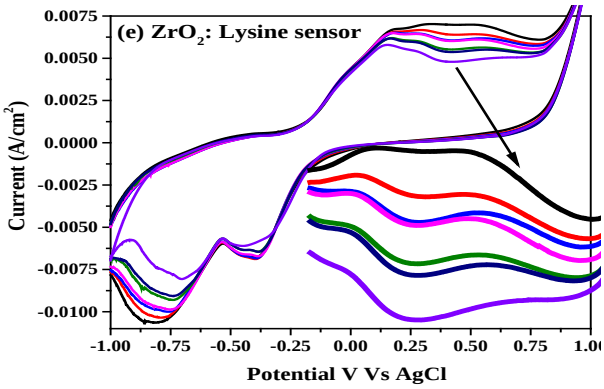

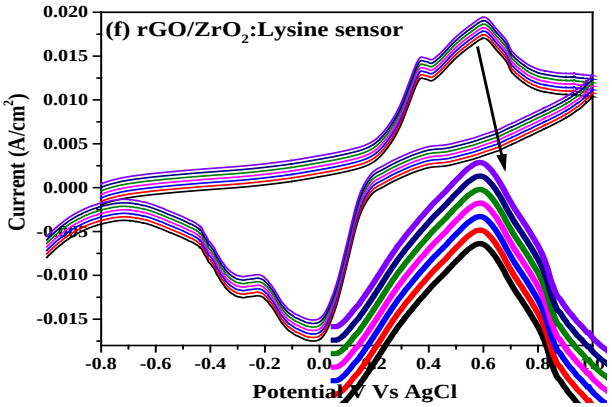

Figure 9. (a, c) CV graph (b, d) Calibration curve (e, f) CV response of Lysine through ZrO_2 and ZrO_2/rGO.

CONCLUSION

The synthesized ZrO_2 and ZrO_2/rGO was confirmed using spectroscopic techniques and evaluated for its biological and electrochemical studies. The biological performance of ZrO_2/rGO nanocomposite was significantly enhanced against *Penicillium sp.* and *Aspergillus Niger and* antioxidant property shown 82 % with an IC_{50} value of 31 mg/mL. Also, the electrochemical studies confirmed the better capacitance value and sensing property using ZrO_2 wrapped by rGO nanocomposite.

AUTHOR CONTRIBUTION STATEMENT

Sanjeevarayappa C: Experimental, Data Collection, Nagegowda P: Visualization, Mylarappa M: Supervision Chandruvasan S: review and editing Sandhya R: Characterization Techniques, Prasanna Kumar S G: Investigation.

DECLARATION OF COMPETING INTEREST

The authors declare that they have no known competing financial interests or personal relationships that could have appeared to influence the work reported in this paper.

REFERENCES

1. H. Dong, Y. Li, J. Yu, et al. A Versatile Multicomponent Assembly via β-cyclodextrin Host–Guest Chemistry on Graphene for Biomedical Applications. *Small* **2013**, 9 (3), 446–456.
2. C. Gardin, A. Piattelli, B. Zavan. Graphene in Regenerative Medicine: Focus on Stem Cells and Neuronal Differentiation. *Trends in Biotechnology* **2016**, 34 (6), 435–437.
3. G. Reina, E. Tamburri, S. Orlanducci, et al. Nanocarbon surfaces for biomedicine. *Biomatter* **2014**, 4 (1), e28537.
4. T. Zhou, X. Zhou, D. Xing. Controlled release of doxorubicin from graphene oxide based charge-reversal nanocarrier. *Biomaterials* **2014**, 35 (13), 4185–4194.
5. V.C. Sanchez, A. Jachak, R.H. Hurt, A.B. Kane. Biological Interactions of Graphene-Family Nanomaterials: An Interdisciplinary Review. *Chem. Res. Toxicol.* **2012**, 25 (1), 15–34.
6. Y. Zhang, S.F. Ali, E. Dervishi, et al. Cytotoxicity Effects of Graphene and Single-Wall Carbon Nanotubes in Neural Phaeochromocytoma-Derived PC12 Cells. *ACS Nano* **2010**, 4 (6), 3181–3186.
7. Y. Li, Y. Liu, Y. Fu, et al. The triggering of apoptosis in macrophages by pristine graphene through the MAPK and TGF-beta signaling pathways. *Biomaterials* **2012**, 33 (2), 402–411.
8. O. Akhavan, E. Ghaderi, A. Akhavan. Size-dependent genotoxicity of graphene nanoplatelets in human stem cells. *Biomaterials* **2012**, 33 (32), 8017–8025.
9. Y. Sun, H. Dai, S. Chen, et al. Graphene oxide regulates *cox2* in human embryonic kidney 293T cells via epigenetic mechanisms: dynamic chromosomal interactions. *Nanotoxicology* **2018**, 12 (2), 117–137.
10. S. Kumar, J.G. Sharma, S. Maji, B.D. Malhotra. Nanostructured zirconia decorated reduced graphene oxide based efficient biosensing platform for non-invasive oral cancer detection. *Biosensors and Bioelectronics* **2016**, 78, 497–504.
11. B. Liu, J. Hu, J.S. Foord. Electrochemical Deposition of Zirconia Films on Diamond Electrodes. *Electrochem. Solid-State Lett.* **2011**, 14 (2), D20.
12. G. Poungchan, B. Ksapabutr, M. Panapoy. One-step synthesis of flower-like carbon-doped ZrO_2 for visible-light-responsive photocatalyst. *Materials & Design* **2016**, 89, 137–145.
13. J. Zhang, L. Li, D. Liu, et al. Multi-layer and open three-dimensionally ordered macroporous TiO_2–ZrO_2 composite: diversified design and the comparison of multiple mode photocatalytic performance. *Materials & Design* **2015**, 86, 818–828.
14. M. M, R. S, K. S, C. S, S. K N. Synthesis and Characterization of ZnO and MgO Nanoparticles through Green Approach and Their Antioxidant Properties. *ECS Trans.* **2022**, 107 (1), 689–695.
15. V. Sai Saraswathi, N. Kamarudheen, K.V. BhaskaraRao, K. Santhakumar. Phytoremediation of dyes using Lagerstroemia speciosa mediated silver nanoparticles and its biofilm activity against clinical strains Pseudomonas aeruginosa. *Journal of Photochemistry and Photobiology B: Biology* **2017**, 168, 107–116.
16. F. Liu, J. Kim, Y. Li, et al. An Extract of Lagerstroemia speciosa L. Has Insulin-Like Glucose Uptake–Stimulatory and Adipocyte Differentiation–Inhibitory Activities in 3T3-L1 Cells. *The Journal of Nutrition* **2001**, 131 (9), 2242–2247.
17. M. Mylarappa, S. Chandruvasan, K.S. Harisha, et al. Development of Coriander Honey loaded CeO_2 for cyclic voltammetry, chemical sensor, dye purification, and antioxidant properties. *Journal of the Taiwan Institute of Chemical Engineers* **2023**, 152, 105174.
18. N.K. Mogha, V. Sahu, M. Sharma, R.K. Sharma, D.T. Masram. Biocompatible ZrO_2- reduced graphene oxide immobilized AChE biosensor for chlorpyrifos detection. *Materials & Design* **2016**, 111, 312–320.
19. V. Sai Saraswathi, K. Santhakumar. Photocatalytic activity against azo dye and cytotoxicity on MCF-7 cell lines of zirconium oxide nanoparticle mediated using leaves of Lagerstroemia speciosa. *Journal of Photochemistry and Photobiology B: Biology* **2017**, 169, 47–55.
20. S. Balaji, B.K. Mandal, S. Ranjan, N. Dasgupta, R. Chidambaram. Nano-zirconia – Evaluation of its antioxidant and anticancer activity. *Journal of Photochemistry and Photobiology B: Biology* **2017**, 170, 125–133.
21. I.I.C. Chio, D.A. Tuveson. ROS in Cancer: The Burning Question. *Trends in Molecular Medicine* **2017**, 23 (5), 411–429.
22. M. Mylarappa, S. Chandruvasan, K.S. Harisha, K.N. Shravana Kumara. Ajwain honey loaded CeO_2 nanocomposite for antioxidant, chemical sensors and photocatalysis studies. *Kuwait Journal of Science* **2024**, 51 (1), 100145.
23. H. Zhang, B. Chen, H. Jiang, et al. A strategy for ZnO nanorod mediated multi-mode cancer treatment. *Biomaterials* **2011**, 32 (7), 1906–1914.
24. A. Abdal Dayem, M. Hossain, S. Lee, et al. The Role of Reactive Oxygen Species (ROS) in the Biological Activities of Metallic Nanoparticles. *IJMS* **2017**, 18 (1), 120.
25. A.T. Ezhil Vilian, M. Rajkumar, S.-M. Chen. In situ electrochemical synthesis of highly loaded zirconium nanoparticles decorated reduced graphene oxide for the selective determination of dopamine and paracetamol in presence of ascorbic acid. *Colloids and Surfaces B: Biointerfaces* **2014**, 115, 295–301.
26. M. Mylarappa, S. Chandruvasan, K.S. Harisha, S.C. Sharath. Synthesis, characterization and electrochemical detection of tartaric acid and grape juice using rGO doped La_2O_3 nanoparticles. *Materials Science and Engineering: B* **2024**, 299, 116977.
27. S. Rani, M. Kumar, S. Sharma, D. Kumar, S. Tyagi. Effect of Graphene in Enhancing the Photo Catalytic Activity of Zirconium Oxide. *Catal Lett* **2014**, 144 (2), 301–307.

28. S. Gurunathan, J.W. Han, J.H. Park, J.-H. Kim. An in vitro evaluation of graphene oxide reduced by Ganoderma spp. in human breast cancer cells (MDA-MB-231). *Int J. Nanomed.* **2014**, 1783.
29. M. M, C. S, K. S, R. S. Synthesis and Characterization of Rgo Doped Nb_2O_5 Nano Composite for Chemical Sensor Studies. *ECS Trans.* **2022**, 107 (1), 269–275.
30. M. Mylarappa, S. Chandruvasan, R. Sandhya. Development of rGO/RuO_2 nanocomposite for voltammetric sensors, dye degradation and antioxidant studies. *Materials Chemistry and Physics* **2024**, 316, 129104.
31. M. Mylarappa, S. Kantharaju, V. Suchithra, et al. Development of Illite modified/Rh_2O_3 for electrochemical, sensor, photocatalysis and antioxidant studies. *Applied Clay Science* **2024**, 252, 107330.
32. M. Kaur, K. Pal. An investigation for hydrogen storage capability of zirconia-reduced graphene oxide nanocomposite. *Int. J. Hydrogen Energy* **2016**, 41 (47), 21861–21869.
33. M. Mylarappa, C. Selvam, H.K. Sanjeevappa, et al. Reduced graphene oxide loaded La_2O_3 nanocomposite for dye degradation and antioxidant studies. *Results in Surfaces and Interfaces* **2024**, 14, 100202.
34. J. Hu, F. Yang, C. Lai, et al. Researches on a conductive polyaniline-acetylene black composite to suppress the hydrogen evolution reaction in lead-acid batteries. *J Solid State Electrochem* **2022**, 26 (5), 1153–1161.
35. N. Swetha, V. Venkata Lakshmi, M. Mylarappa, S. Chandruvasan, K.S. Harisha. Development of SiO_2/rGO from Rice Husk for Photocatalysis, Antioxidant, Electrochemical and Green Sensor Detection Studies. *Silicon* **2024**.
36. A.M. Bannunah. Biomedical Applications of Zirconia-Based Nanomaterials: Challenges and Future Perspectives. *Molecules* **2023**, 28 (14), 5428.
37. S. Mb, M. C., S. M., et al. Development of $NiCoO_2$ Nanoparticles based Electrochemical Sensor with Extremely Low Detection for Hazardous 4-Nitrophenol. *J. Electrochem. Soc.* **2023**, 170 (6), 067509.
38. M. Mylarappa, S. Chandruvasan, K.S. Harisha, et al. Green synthesis of natural gomutra and honey doped CeO_2 nanocomposite for green sensor, cyclic voltammetry, photocatalysis and antioxidant studies. *Green Technologies and Sustainability* **2024**, 2 (2), 100085.
39. S. Kota, S. Chandruvasan, A. Shivashankar, A.I. Mab, R. Annapragada. A review on the synthesis and characterization of MXene and electrochemical sensor of dopamine and glucose. *Ionics* **2024**.
40. S. Chandruvasan, H. Madival, M. Mylarappa, et al. Investigation of Antioxidant and Photo Catalysis of Natural Honey and Cow Urine-Doped CeO_2 Nanoparticles Fabricated by Reflux Method. In *Engineering, Science, and Sustainability*; CRC Press, London, **2023**; pp 31–36.